

Scaling Laws for Black-box Adversarial Attacks

Chuan Liu^{1,2,3*} Huanran Chen^{1,3*} Yichi Zhang^{1,3} Jun Zhu^{1,3} Yinpeng Dong^{1,3}

¹ Dept. of Comp. Sci. and Tech., Institute for AI, Tsinghua-Bosch Joint ML Center, THBI Lab, BNRist Center, Tsinghua University, Beijing, 100084, China

² IIS, Tsinghua University ³ RealAI

{liuchuan22, zyc22}@mails.tsinghua.edu.cn, huanran.chen@outlook.com

{dongyinpeng, dcszj}@mail.tsinghua.edu.cn

Abstract

Adversarial examples exhibit cross-model transferability, enabling threatening black-box attacks on commercial models. Model ensembling, which attacks multiple surrogate models, is a known strategy to improve this transferability. However, prior studies typically use small, fixed ensembles, which leaves open an intriguing question of whether scaling the number of surrogate models can further improve black-box attacks. In this work, we conduct the first large-scale empirical study of this question. We show that by resolving gradient conflict with advanced optimizers, we discover a robust and universal log-linear scaling law through both theoretical analysis and empirical evaluations: the Attack Success Rate (ASR) scales linearly with the logarithm of the ensemble size T . We rigorously verify this law across standard classifiers, SOTA defenses, and MLLMs, and find that scaling distills robust, semantic features of the target class. Consequently, we apply this fundamental insight to benchmark SOTA MLLMs. This reveals both the attack’s devastating power and a clear robustness hierarchy: we achieve 80%+ transfer attack success rate on proprietary models like GPT-4o, while also highlighting the exceptional resilience of Claude-3.5-Sonnet. Our findings urge a shift in focus for robustness evaluation: from designing intricate algorithms on small ensembles to understanding the principled and powerful threat of scaling.

1. Introduction

Over the past decade, deep learning has achieved remarkable advancements across various computer vision tasks, leading to its widespread applications [39]. However, deep neural networks (DNNs) remain susceptible to adversarial

*Equal contribution.

†Our code is available at <https://github.com/liuchuan22/ScaleUpAttack>.

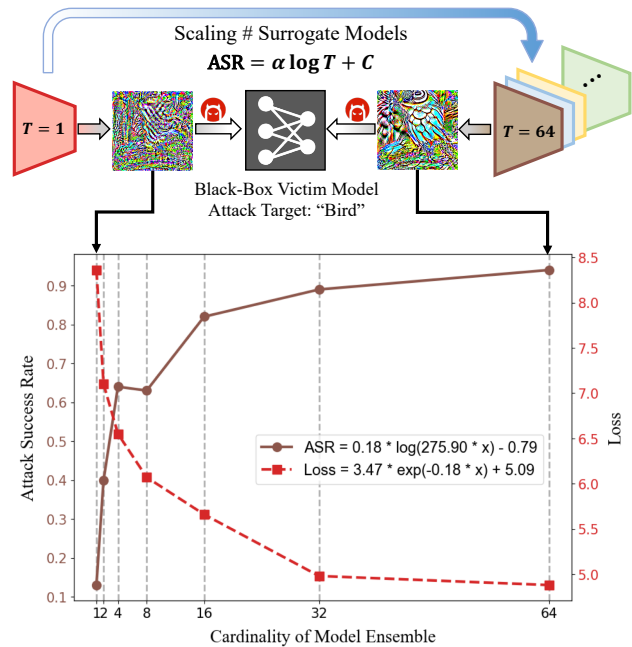


Figure 1. Key observation of scaling laws for the transfer-based black-box attack. By scaling the number of surrogate models in the ensemble, we observe that the attack success rate and the discriminative loss on the target model follow a log-linear scaling law.

examples [26, 57] – perturbations that are subtle and nearly imperceptible but can significantly mislead the model, resulting in incorrect predictions. Adversarial attacks have garnered considerable interest due to their implications for understanding DNN functionality [14], assessing model robustness [73], and informing the development of more secure algorithms [50].

Adversarial attacks are typically categorized into white-box and black-box attacks based on whether the attacker has knowledge of the architecture and parameters of the target model. Given the greater risks with commercial services, e.g., GPT-4 [53], black-box attack methodologies [15, 45]

have attracted growing attention. One prominent approach within black-box attacks is the transfer-based attack, which approximately optimizes the adversarial examples against the black-box model by minimizing the discriminative loss on a selection of predefined surrogate models. Researchers have devised advanced optimization algorithms [42, 50, 61] and data augmentation techniques [16, 48] in transfer-based attacks. Model ensembling [15, 45] further facilitates these methods by leveraging multiple surrogate models simultaneously to improve the transferability of adversarial examples. By averaging the gradients or predictions from different models, ensemble attack methods seek to increase the transferability across various target models [8, 15].

Despite the progress in ensemble attack algorithms, the number of surrogate models used in previous research is often limited [8, 70, 72]. Recent advancement in large language models shows that scaling training data can significantly improve the generalization ability [34]. Since the transfer-based attack is also a generalization problem that expects adversarial examples from surrogate models to generalize to target models, while the training data are surrogate models rather than text or images [8, 15], this equivalence prompts an intriguing question: *Can we achieve significant improvements in transfer-based attacks by scaling the number of surrogate models, akin to the scaling of data and model parameters in large language models like GPT?*

In this work, we conduct the first large-scale empirical investigation into the scaling laws of black-box adversarial attacks, given that the gradient conflict issue is properly resolved (Sec. 2.2). Our central finding is the discovery of a robust and universal log-linear scaling law: the Attack Success Rate (ASR) on black-box targets scales linearly with the logarithm of the ensemble cardinality T . We provide an asymptotic analysis on the convergence rate of generation error and adversarial examples under idealized IID assumptions (Sec. 3.1). Our core contribution, however, is the empirical discovery and verification of the precise log-linear form of these scaling laws (Sec. 3.3). We rigorously demonstrate the universality of these scaling laws across diverse target families (Sec. 3.4), and provide a qualitative explanation for this phenomenon (Sec. 5.2): as T increases, the optimizer is forced to discard model-specific, non-robust features and instead learns the robust, semantic features of the target class, resulting in highly transferable perturbations.

Inspired by this fundamental insight, we then extend our scaling laws to attack the foundational vision encoders (e.g., CLIP) of modern MLLMs (Sec. 4) to demonstrate its practical power as both a SOTA attack and a novel robustness benchmark. We achieve devastatingly high ASR on top-tier models, including 90.0% ASR on Qwen3-VL-235B and 85.0% ASR on GPT-4o. Meanwhile, our scaling benchmark reveals a stark hierarchy in SOTA model robustness. We highlight the exceptional resilience of Claude-3.5-

Sonnet in sharp contrast to the high vulnerability of Gemini-2.5-Pro. These findings show that scaling is a critical, measurable threat vector, and we urge the community to adopt large-scale robustness evaluation, rather than designing intricate algorithms on small ensembles, to build and validate genuinely robust and trustworthy foundation models.

2. Backgrounds

In this section, we provide necessary backgrounds, including the problem formulations for different attack settings and the prerequisite algorithms.

2.1. Problem Formulations

Our work investigates scaling laws across multiple black-box attack scenarios. We formulate the settings below.

2.1.1. Attacks on Image Classifiers

Let \mathcal{F} denote the set of all image classifiers. The vulnerability of such classifiers to adversarial examples has been a long-standing area of research [26, 57]. Given a natural image \mathbf{x}_{nat} with its true label \mathbf{y}_{nat} , the goal of a transfer-based attack is to craft an adversarial example \mathbf{x} within an ℓ_∞ perturbation budget ϵ that fools black-box target models.

Targeted Attack. The primary focus of our work is the challenging targeted attack setting. Given a target class \mathbf{y} (where $\mathbf{y} \neq \mathbf{y}_{\text{nat}}$), the goal is to craft an \mathbf{x} that is misclassified as \mathbf{y} . This can be formulated as minimizing the expected loss over all models in \mathcal{F} :

$$\min_{\mathbf{x}} \mathbb{E}_{f \in \mathcal{F}} [\mathcal{L}(f(\mathbf{x}), \mathbf{y})], \quad \text{s.t. } \|\mathbf{x} - \mathbf{x}_{\text{nat}}\|_\infty \leq \epsilon, \quad (1)$$

where \mathcal{L} is a loss function (e.g., cross-entropy). In practice, we approximate this by ensembling a limited set of T surrogate classifiers $\{f_i\}_{i=1}^T \subset \mathcal{F}$:

$$\min_{\mathbf{x}} \frac{1}{T} \sum_{i=1}^T \mathcal{L}(f_i(\mathbf{x}), \mathbf{y}), \quad \text{s.t. } \|\mathbf{x} - \mathbf{x}_{\text{nat}}\|_\infty \leq \epsilon. \quad (2)$$

Untargeted Attack. We also validate our scaling laws in the untargeted setting in Sec. 5.1, where the goal is to mislead the classifier to **any** class other than \mathbf{y}_{nat} . The objective is to maximize the loss with respect to original \mathbf{y}_{nat} :

$$\max_{\mathbf{x}} \frac{1}{T} \sum_{i=1}^T \mathcal{L}(f_i(\mathbf{x}), \mathbf{y}_{\text{nat}}), \quad \text{s.t. } \|\mathbf{x} - \mathbf{x}_{\text{nat}}\|_\infty \leq \epsilon. \quad (3)$$

2.1.2. Attacks on Vision Encoders

Contrastive Language-Image Pretraining (CLIP) is a popular self-supervised framework that can pretrain large-scale language-vision models on web-scale text-image pairs via contrastive learning [38, 54, 55]. Based on the generalization ability of CLIP models, previous works have utilized them as surrogate models in model ensembles [1, 19, 23].

We extend our analysis to attack these vision encoders, which are foundational to modern MLLMs. Instead of classifying to a specific logit, the goal is to craft an image \mathbf{x} whose embedding $f^I(\mathbf{x})$ is close to the text embedding \mathbf{e}_{tar} of a target label \mathbf{y} . This target embedding is typically pre-computed using a text encoder, f^T . The objective function is adapted by replacing the classifier f_i with a surrogate image encoder f_i^I and the cross-entropy loss \mathcal{L} with a similarity-based loss \mathcal{L}_{sim} (e.g., cosine embedding loss):

$$\min_{\mathbf{x}} \frac{1}{T} \sum_{i=1}^T \mathcal{L}_{\text{sim}}(f_i^I(\mathbf{x}), \mathbf{e}_{\text{tar}}), \quad \text{s.t. } \|\mathbf{x} - \mathbf{x}_{\text{nat}}\|_{\infty} \leq \epsilon, \quad (4)$$

where $\mathbf{e}_{\text{tar}} = f^T(\mathbf{y})$ is the fixed target text embedding.

2.2. Prerequisite Algorithms

Researchers have developed sophisticated algorithms to enhance adversarial transferability, which can be categorized into gradient optimizers, input transformations, and ensemble strategies.

2.2.1. Gradient Optimizers

These methods refine the gradient update step itself. A pioneering example is **MI-FGSM** [15], which stabilizes gradients by integrating a momentum term:

$$\mathbf{g}_{t+1} = \mu \cdot \mathbf{g}_t + \frac{\nabla_{\mathbf{x}} \mathcal{L}(\mathbf{x}_t, \mathbf{y})}{\|\nabla_{\mathbf{x}} \mathcal{L}(\mathbf{x}_t, \mathbf{y})\|_1}, \quad (5)$$

with update $\mathbf{x}_{t+1} = \mathbf{x}_t + \alpha \cdot \text{sign}(\mathbf{g}_{t+1})$. Other methods like **VMI-FGSM** [61] further refine this momentum concept.

2.2.2. Input Transformations

These methods apply data augmentation during the attack to find more generalizable adversarial patterns. Prominent examples include Diverse Inputs (DI) [66] and Spectrum Simulation Attack (SSA) [48]. SSA, a state-of-the-art method, applies spectrum transformations \mathcal{T} and computes gradients on the transformed input $\mathcal{T}(\mathbf{x})$.

2.2.3. Ensemble Strategies and Gradient Conflict

The above components can be applied to ensemble attacks. The most straightforward method, often used with MI-FGSM, is logit ensembling [15], where the optimizer computes gradients over the sum of all models' logits.

While simple, this strategy exposes a critical flaw: **gradient conflict**. We discover that as the number of surrogates (T) increases, the gradients from different models, which often lack semantics and have random directions, tend to cancel each other out. As shown in Fig. 2, this conflict causes the ensemble gradient norm to collapse, leading to complete optimization stagnation.

To address this, advanced optimizers are required. These methods aim to find a common direction of vulnerability

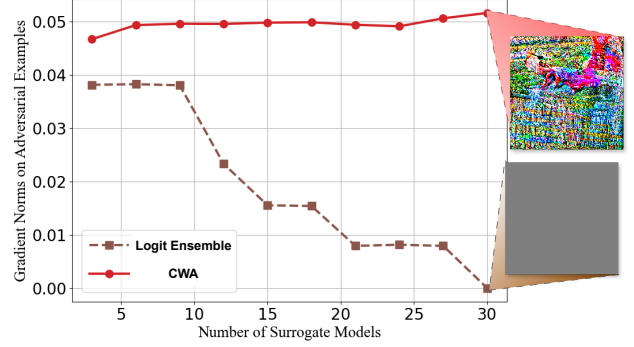


Figure 2. Comparisons between CWA and a naïve ensemble (MI-FGSM with logit averaging). As T increases, the naïve method suffers optimization stagnation (gradient norm collapses) due to gradient conflict. Advanced methods like CWA, which align gradients, avoid this issue entirely.

rather than simply averaging gradients. They typically work by reducing gradient variance, such as SVRE [68], or by encouraging gradient alignment, which is the approach taken by the Common Weakness Attack (CWA) [8]. CWA seeks common vulnerabilities by encouraging flatter loss landscapes and minimizing the second-order Taylor series:

$$\frac{1}{T} \sum_{i=1}^T \left[\mathcal{L}(f_i(\mathbf{p}_i, \mathbf{y})) + \frac{1}{2} (\mathbf{x} - \mathbf{p}_i)^\top H_i (\mathbf{x} - \mathbf{p}_i) \right], \quad (6)$$

where \mathbf{p}_i is the closest optimum of model f_i to \mathbf{x} and H_i is the Hessian. As Fig. 2 demonstrates, CWA effectively avoids the optimization stagnation seen in MI-FGSM.

Our Chosen Algorithm: SSA-CWA. For our main experiments, we require an algorithm that both resolves the gradient conflict and achieves state-of-the-art performance. We therefore select SSA-CWA, which combines the advanced input transformation of SSA [48] with the robust gradient optimization of CWA [8] (pseudocode provided in Appendix C). While leveraging SSA-CWA as our core algorithm, we also explore the scaling laws of other optimizers and validate our gradient conflict hypothesis in Sec. 5.1.

3. Scaling Laws for Adversarial Attacks

In this section, we present our key findings on scaling laws for black-box adversarial attacks. Sec. 3.1 introduces the theoretical motivation for our study. Sec. 3.2 details our experimental setup for generating adversarial examples. Sec. 3.3 presents the initial discovery of the empirical scaling laws on standard classifiers. Finally, Sec. 3.4 verifies the universality of these laws by testing them against state-of-the-art defended models and across diverse MLLMs.

3.1. Motivation

First, we observe that in most practical scenarios, \mathbf{x}_{nat} and \mathbf{y} are predefined and fixed. Consequently, Eq. (1) and Eq. (2)

can be considered as functions of variable \mathbf{x} only.

Definition 1. Define \mathbf{x}^* and $\hat{\mathbf{x}}$ to be the minimizers of Eq. (1) and Eq. (2), respectively, which can be written as

$$\begin{aligned}\mathbf{x}^* &= \arg \min_{\mathbf{x}} \mathbb{E}_{f \in \mathcal{F}} [\mathcal{L}(f(\mathbf{x}), \mathbf{y})], \\ \hat{\mathbf{x}} &= \arg \min_{\mathbf{x}} \frac{1}{T} \sum_{i=1}^T \mathcal{L}(f_i(\mathbf{x}), \mathbf{y}),\end{aligned}\quad (7)$$

with the same ℓ_∞ norm constraints given in Eq. (1) and (2).

Definition 2. Define $\mathbb{L}(\cdot)$ as the population loss in Eq. (1), and $\mathbb{L}(f_i(\cdot))$ as the loss on one surrogate model f_i :

$$\begin{aligned}\mathbb{L}(\mathbf{x}) &= \mathbb{E}_{f \in \mathcal{F}} [\mathcal{L}(f(\mathbf{x}), \mathbf{y})], \\ \mathbb{L}(f_i(\mathbf{x})) &= \mathcal{L}(f_i(\mathbf{x}), \mathbf{y}).\end{aligned}\quad (8)$$

These definitions are used to simplify our notations and better demonstrate our proofs. Then, we bring our key observations that are shown in the following theorem.

Theorem 1. Suppose that model ensemble $\{f_i\}_{i=1}^T$ is i.i.d. sampled from some distribution on \mathcal{F} , and $\hat{\mathbf{x}}$ goes to \mathbf{x}^* as $T \rightarrow \infty$. Denote \xrightarrow{d} as convergence in distribution, and Cov as the covariance matrix. Then we have the following asymptotic bound as $T \rightarrow \infty$:

$$\begin{aligned}\sqrt{T}(\hat{\mathbf{x}} - \mathbf{x}^*) &\xrightarrow{d} \mathcal{N}(0, (\nabla^2 \mathbb{L}(\mathbf{x}^*))^{-1} \text{Cov}(\mathbb{L}(f_i)) (\nabla^2 \mathbb{L}(\mathbf{x}^*))^{-1}), \\ T(\mathbb{L}(\hat{\mathbf{x}}) - \mathbb{L}(\mathbf{x}^*)) &\xrightarrow{d} \frac{1}{2} \|S\|_2^2, \text{ with} \\ S &\sim \mathcal{N}(0, (\nabla^2 \mathbb{L}(\mathbf{x}^*))^{1/2} \text{Cov}(\mathbb{L}(f_i)) (\nabla^2 \mathbb{L}(\mathbf{x}^*))^{1/2}).\end{aligned}\quad (9)$$

Proof of Theorem 1 can be found in Appendix A.

Remark 1. Theorem 1 suggests that the adversarial examples converge in $\mathcal{O}(\frac{1}{\sqrt{T}})$, while the difference between population loss and empirical loss converges in $\mathcal{O}(\frac{1}{T})$.

When we replace \mathcal{L} with the cross-entropy loss in Theorem 1, we obtain Theorem 2 by some simple derivations.

Theorem 2. Following the notation and assumptions in Theorem 1, when using the cross-entropy loss, we have:

$$\begin{aligned}\sqrt{T}(\hat{\mathbf{x}} - \mathbf{x}^*) &\xrightarrow{d} \mathcal{N}(0, (\nabla^2 \mathbb{L}(\mathbf{x}^*))^{-1}), \\ T(\mathbb{L}(\hat{\mathbf{x}}) - \mathbb{L}(\mathbf{x}^*)) &\xrightarrow{d} \frac{1}{2} \|\mathcal{N}(0, \mathbf{I})\|_2^2.\end{aligned}\quad (10)$$

Remark 2. Theorem 2 holds since $\text{Cov}(\mathbb{L}(f_i(\mathbf{x}^*))) = \nabla^2 \mathbb{L}(\mathbf{x}^*)$ for the cross-entropy loss. Therefore, we have $2T(\mathbb{L}(\hat{\mathbf{x}}) - \mathbb{L}(\mathbf{x}^*)) \xrightarrow{d} \chi^2(D)$ where D is the dimension of the input, which means $\mathbb{L}(\hat{\mathbf{x}}) - \mathbb{L}(\mathbf{x}^*)$ converges in $\mathcal{O}(\frac{D}{2T})$.

These theorems provide the core theoretical motivation for our work: increasing the ensemble cardinality T is a principled approach, as it provably closes the gap between the empirical loss and the true population loss. However, we must acknowledge a crucial gap between theory and practical setting of black-box attacks. The theorems rely on i.i.d. assumptions that are not met in practice but for a theoretical convenience. In practice, our surrogate models are typically pre-trained on similar datasets (e.g., ImageNet) and share strong architectural biases, making them highly correlated [32]. Consequently, the asymptotic $\mathcal{O}(1/T)$ convergence rate derived in Remark 2 is unlikely to hold.

Therefore, we posit that while the theory provides a strong *qualitative* motivation (i.e., scaling T should improve transferability), it does not offer a *quantitative prediction* for the *empirical* scaling law. The central question of how ASR and loss actually behave as T increases in a practical setting remains open. This motivates our large-scale empirical investigation in the following sections to discover the true scaling laws governing black-box attacks.

3.2. Experimental Setup

To investigate the relationship between the number of surrogate models and attack efficacy, we first define our comprehensive experimental setup. This setup is used to generate a single, fixed set of adversarial examples, which are then evaluated across diverse target models to discover and verify our proposed scaling laws.

3.2.1. Adversarial Example Generation

Surrogate Pool. To ensure the transferability and diversity of our attack, we select a large pool of 64 models from Torchvision [51] and Timm [63]. This pool includes a wide variety of architectures, hyperparameters, and training datasets, such as AlexNet [36], DenseNet [29], EfficientNet [58], ResNet [27], ViT [20], DeiT [59], and many others. The full list is available in Appendix B.

Ensemble Sampling and Attack Algorithm. We generate adversarial examples by attacking ensembles of surrogate models. For each attack, an ensemble is constructed by randomly sampling T models from our 64-model pool. We vary the ensemble cardinality T across a logarithmic scale from 2^0 to 2^6 . We use the SSA-CWA attack [8] for 40 iteration steps, with a perturbation budget of $\epsilon = 8/255$ under the ℓ_∞ norm. The loss function \mathcal{L} is the standard cross-entropy loss. This process yields 7 distinct sets of adversarial examples, one for each value of T .

3.2.2. Target Model Families

To test the universality of any observed scaling phenomena, we evaluate our pre-generated adversarial examples against three distinct families of black-box target models:

- **Family 1: Standard Image Classifiers.** We select 7 widely-used models, including Swin-Transformers [46],

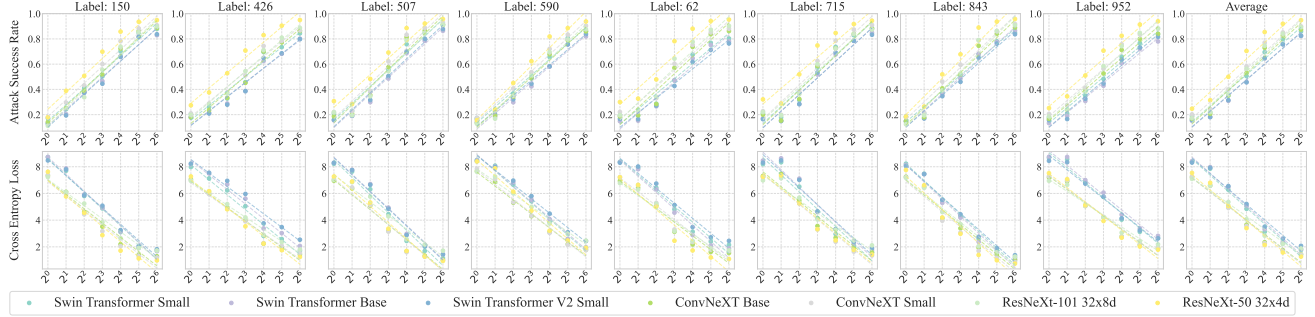


Figure 3. Scaling Laws over model ensemble in a black-box setting. We plot the x-axis on a base-2 logarithmic scale, and we measure both the attack success rate (ASR) and average cross entropy-loss of target models. The cardinality of the model ensembles is varied from 2^0 to 2^6 , with models randomly selected for each ensemble. We fit the results of selected target models by lines for better demonstration.

ConvNeXt [47], and ResNeXt [67].

- **Family 2: Defended Models.** We select 6 models representing SOTA defenses, including adversarially trained models (FGSMAT [37], EnsAT [60]) and purification defenses (HGD [41], BDR [17], JPEG, and DiffPure [52]).
- **Family 3: Multimodal Large Language Models.** We select 3 popular MLLMs: LLaVA-1.5-7B [43], Qwen-2.5-VL-7B [4], and Llama-3.2-11B-Vision*. These are used to further *validate the generality* of the laws across different data modalities and architectures.

3.2.3. Dataset and Evaluation Metrics

Dataset and Generation Protocol. Following previous work, we leverage the 1000 images from the ImageNet-1K NIPS 2017 dataset [33, 69]. To ensure the generality of our findings and create a large-scale testbed, we target 8 distinct categories for each source image [71]. This creates a total of $1000 \times 8 = 8000$ unique source-target pairs for each ensemble configuration. As we generate adversarial examples for 7 distinct ensemble cardinalities $T \in \{2^0, 2^1, \dots, 2^6\}$, this results in a large-scale dataset of $7 \times 8000 = 56000$ generated adversarial examples.

To ensure our results are statistically robust and not biased by a single ‘lucky’ or ‘unlucky’ random selection of surrogate models, we employ a batched generation protocol. For any given cardinality T , we first partition the 1000 source images into 8 disjoint batches of 125 images. Then, for each batch, we randomly sample a *new* ensemble of T models from our surrogate pool. This newly sampled ensemble is used to craft the 125 adversarial examples (against all 8 target classes) for its assigned batch. This methodology ensures that the final metrics for each T are averaged over 8 distinct, randomly-drawn ensembles, providing a highly robust and generalizable measurement of the scaling effect.

Metrics. For Family 1 and 2, we measure the Attack Success Rate (ASR), which is defined by the ratio between number of successful attacks (misclassified as target label)

and total number of attacks. We also record the cross entropy loss between classifiers’ predictions and target labels for Family 1 to demonstrate the validity of using ASR as the measurements of transferability. For Family 3 (MLLMs), which output text, we adopt a simple evaluation paradigm by string matching the target label text (e.g., ‘sea lion’ for target label 150) and the MLLMs’ descriptions. Since MLLMs produce descriptive text rather than precise classification results, we therefore adopt a relaxed keyword map (provided in Appendix D) to more robustly identify any semantic mentions of the target concept within the outputs.

3.3. Log-Linear Scaling Laws in Image Classifiers

3.3.1. Empirical Observation

We begin our analysis by evaluating the generated adversarial examples on the standard image classifiers. As demonstrated in Fig. 3 (top row), we identify a robust empirical phenomenon: the attack success rate (ASR) exhibits strong *log-linear scaling laws* with the ensemble cardinality T .

As shown by the fitted lines, the ASR increases linearly as we increase T on a logarithmic scale. Concurrently, the average cross-entropy loss against the target label (top row of Fig. 3) exhibits a mirrored log-linear decay. This strong symmetric relationship confirms that ASR is a valid and robust proxy for the true optimization objective, as the decreasing loss directly correlates with the increasing success rate. This suggests that the effectiveness of ensemble attacks scales in a highly predictable manner, where each doubling of T yields a consistent improvement in ASR.

3.3.2. Analysis of the Log-Linear Relationship

We empirically analyze the observable characteristics of these log-linear scaling laws:

- **The Intercept (Baseline Vulnerability):** The starting point of the line (at $T = 1$) represents the model’s baseline vulnerability to single-model transfer attacks. As seen in Fig. 3, this intercept is influenced by various factors, including the target model’s architecture and the specific adversarial target.

*<https://ai.meta.com/blog/llama-3-2-connect-2024-vision-edge-mobile-devices/>

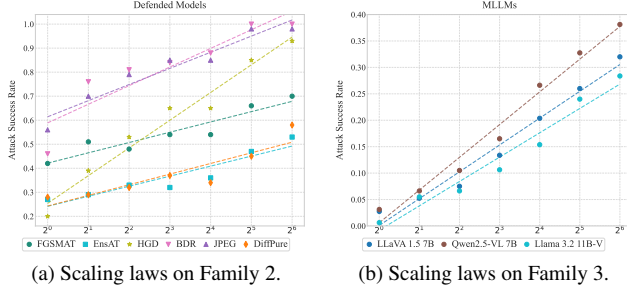


Figure 4. Verification of the log-linear scaling laws’ universality. (a) The trend persists against SOTA defenses. (b) The trend persists for MLLMs. In both settings, we record the ASR averaged across all 8 target classes to show overall model robustness.

- **The Slope (Scaling Efficiency):** The slope of the fitted line represents the ‘scaling efficiency’ of the attack. It quantifies how much ASR is gained for each *doubling* of T . Our results suggest this slope is a key characteristic of the target model’s robustness to scaled attacks.
- **Domain of Validity:** Our observed scaling laws hold true within a specific domain. When T is small ($2^0, 2^1$), the measured ASR shows large variance depending on the specific models randomly selected. The stable log-linear law emerges as a statistical result as T increases. Meanwhile, as ASR approaches 1.0, the metric becomes saturated, and the linear trend naturally flattens. Our observations hold when ASR is below this saturation threshold.

3.4. Verification of the Scaling Laws’ Universality

Having established the existence of these log-linear scaling laws, we now test their universality. A critical question is whether this trend is a fragile artifact of standard classifiers or a more fundamental principle of transfer attacks. We test this by evaluating their robustness against active defenses (Family 2) and their generality across entirely different architectures and modalities (Family 3).

3.4.1. Robustness Against Defended Models

We first test the adversarial examples against the defended models (Family 2). The key question is whether SOTA defenses can ‘break’ this observed scaling trend.

As demonstrated in Fig. 4a, the log-linear scaling laws remain robustly intact. While some defenses successfully lower the overall ASR (seen in the lower ASR values across all T), they *do not* eliminate the fundamental, predictable relationship between $\log T$ and ASR.

This is a critical insight: defenses do not break the underlying scaling behavior. Instead, they primarily increase the ‘cost’ of a successful attack (i.e., requiring a larger T to reach the same ASR). This finding demonstrates that scaling the ensemble is a viable path to breaking even SOTA defenses. By leveraging these scaling laws, we improved the ASR of DiffPure [52] by over 30%, adversarially trained models by over 20%, and HGD [41] by over 50%.

3.4.2. Generalization Across Architectures

Finally, we perform the ultimate test of generality: do the adversarial examples, generated *only* from standard image classifiers, follow the same scaling laws on MLLMs?

Remarkably, as shown in Fig. 4b, the log-linear scaling laws persist even in these advanced multimodal models. This cross-modal generalization is non-trivial, as the MLLMs possess vastly different architectures and are trained on different data modalities. This result strongly supports the generality of our scaling laws.

While the log-linear form is general, the specific robustness of each model varies. For instance, LLaVA-1.5-7B and Qwen-2.5-VL-7B have similar parameter counts ($\approx 7B$) and both show high robustness to single-model attacks, yet their averaged ASR curves clearly diverge, indicating different vulnerabilities to scaling. This suggests that the relationship between model scale and adversarial robustness is more complex in MLLMs and challenges the simple ‘model scale = robustness’ narrative [5].

4. Extending Scaling Laws to Vision Encoders

In this section, we test the generality and power of our discovered scaling laws. Having established the log-linear scaling laws on standard classifiers, we now extend our investigation to a more complex and practical domain: attacking modern MLLMs by targeting their foundational vision encoders, such as CLIP [55]. We hypothesize that the same scaling principles hold when using the embedding-space attack formulation defined in Sec. 2.1.2.

4.1. Experimental Setup

We first introduce our settings for attacking pretrained CLIP models and evaluating them on MLLM targets.

Surrogate Models. We select 12 pretrained open-source CLIP models via OpenCLIP [10]. In contrast to previous works that typically use fewer than 4 surrogate models [74], our scaled ensemble (up to $T = 12$) is sufficient to yield robust results. The full model list is in Appendix E.

Target Models. We select 7 state-of-the-art MLLMs as our black-box targets, including 4 commercial models (GPT-4o [53], Claude-3.5-Sonnet[†], Gemini-2.5-Pro [11], Doubao-Seed-1.6[‡]) and 3 state-of-the-art open-source models (Llama-3.2-90B-Vision-Instruct[§], Qwen3-VL-235B-A22B-Instruct[¶], and DeepSeek-VL2 [65]).

[†]<https://www.anthropic.com/news/claude-3-family>
[‡]<https://seed.bytedance.com/en/blog/introduction-to-techniques-used-in-seed1-6>
[§]<https://ai.meta.com/blog/llama-3-2-connect-2024-vision-edge-mobile-devices/>
[¶]<https://qwen.ai/blog?id=99f0335c4ad9ff6153e517418d48535ab6d8afef&from=research.latest-advancements-list>

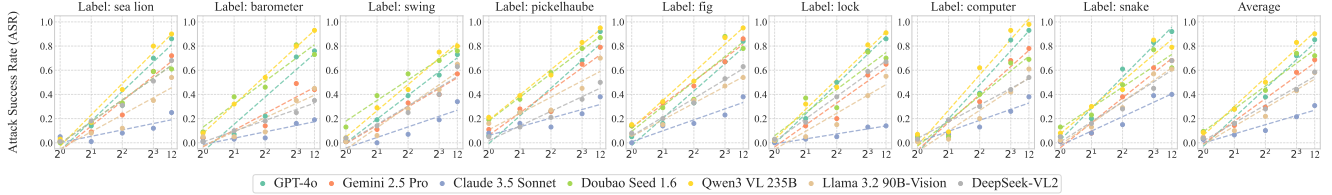


Figure 5. Verification of the log-linear scaling laws on SOTA MLLMs. We use an ensemble of CLIP models as surrogates, scaling the cardinality T from 1 to 12. All attacks in this figure are generated using practical budget ($\epsilon = 16/255$). The ASR is measured using our single, strict LLM-as-Judge metric (defined in Sec. 4.1). The log-linear scaling laws clearly persist.

Dataset and Hyperparameters. We use the same SSA-CWA attack protocol as in Sec. 3.2, but with a simplified dataset for this section. We randomly sample 100 images from the NIPS17 dataset with the same 8 distinct target classes, resulting in 800 unique source-target pairs per ensemble configuration. All experiments in this section are conducted using a unified perturbation budget of $\epsilon = 16/255$ under the ℓ_∞ norm, a common and widely applied setting for practical attacks [19, 49].

Evaluation Metric. We employ a single, unified evaluation metric for all MLLM targets. As MLLMs produce generative outputs instead of classification logits, we adopt the LLM-as-Judge framework from MultiTrust [73]. We leverage GPT-4o to semantically evaluate the target model’s description. An attack is considered successful only if GPT-4 judges that (1) the model’s description mentions the adversarial target concept and (2) the description does not mention factors indicating the image is of low quality, noisy, or modified. The prompt of this strict, high-quality metric is provided in Appendix D.

4.2. Generality and Power of Scaling Laws

Our results, conducted on the latest generation of MLLMs, deliver two key findings.

The log-linear scaling laws persist. Fig. 5 presents the ASR results on our 7 SOTA MLLM targets as a function of ensemble cardinality (T). Our first key finding is that the log-linear scaling laws, discovered in Sec. 3.3, robustly generalize to this new domain. This outcome confirms that the principle is not an artifact of standard classifiers but a fundamental property of ensemble attacks. Even when attacking the complex, SOTA vision encoders of models, scaling the number of CLIP surrogates (T) yields a predictable, linear increase in ASR on a log scale.

Scaling is a powerful and practical weapon. Having verified the scaling laws (Fig. 5), we now examine its practical impact. Table 1 reports the final ASR from our full scaled ensemble ($T = 12$). The results are twofold: they confirm the devastating power of scaling while simultaneously revealing a stark hierarchy in SOTA model robustness. The attack’s power is most evident on Qwen3-VL-235B and GPT-4o, which succumb to a 90.0% and 85.0% average ASR, respectively. This performance rep-

resents a significant leap in practical capability, surpassing the 40-50% ASRs reported by previous methods on commercial models [19]. However, this effectiveness is not universal. Claude-3.5-Sonnet exhibits exceptional robustness, neutralizing the attack to a mere 31.0% ASR. This resilience stands in sharp contrast to its direct competitor, Gemini-2.5-Pro, which is significantly more vulnerable at 69.0% ASR. The open-source landscape mirrors this variability, with DeepSeek-VL2 (59.0%) and Llama-3.2-90B (58.0%) settling into a moderate robustness tier. These results demonstrate that scaling is a powerful and practical tool, and the resulting ASRs serve as a clear benchmark for the diverging robustness of modern MLLMs.

5. Further Analysis and Discussion

In this section, we further demonstrate the robustness of our discovered scaling laws through ablation studies (Sec. 5.1) and provide a deeper analysis into the semantic nature of the perturbations generated via scaling (Sec. 5.2).

5.1. Ablations on the Scaling Laws’ Generality

While our main experiments (Sec. 3) focused on targeted attacks using SSA-CWA, here we verify that the *log-linear scaling laws* are general principles that hold under different attack settings and across various optimizers.

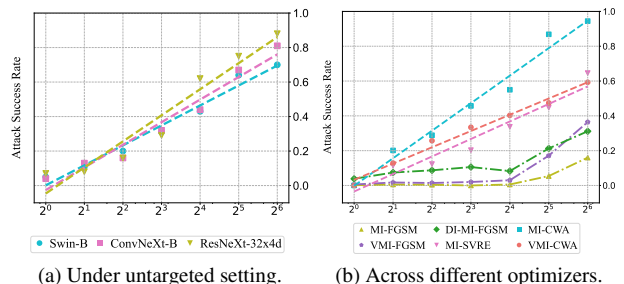


Figure 6. Ablations on the generality of the log-linear scaling laws. (a) The laws persist in the untargeted setting (Eq. 3). (b) The laws hold for advanced optimizers (MI-CWA, VMI-CWA, MI-SVRE) that mitigate gradient conflict. In contrast, the naïve logit ensemble strategy fails to scale, supporting our hypothesis in Sec. 2.2.

Target Model - Label	Sea Lion	Barometer	Swing	Pickelhaube	Fig	Lock	Computer	Snake	Average
GPT-4o	0.86	0.76	0.73	0.92	0.84	0.86	0.93	0.92	0.85
Claude-3.5-Sonnet	0.25	0.19	0.34	0.38	0.38	0.14	0.38	0.41	0.31
Gemini-2.5-Pro	0.72	0.44	0.57	0.79	0.86	0.65	0.78	0.68	0.69
Doubao-Seed-1.6	0.61	0.73	0.76	0.87	0.78	0.70	0.69	0.62	0.72
Llama-3.2-90B-Vision	0.54	0.45	0.65	0.70	0.54	0.55	0.61	0.61	0.58
Qwen3-VL-235B	0.90	0.93	0.80	0.95	0.95	0.91	0.98	0.79	0.90
DeepSeek-VL2	0.68	0.35	0.63	0.50	0.63	0.67	0.54	0.68	0.59

Table 1. Attack Success Rate (ASR) on SOTA MLLMs using our full scaled ensemble ($T = 12$) and practical budget ($\epsilon = 16/255$). The ASR is measured using our unified LLM-as-Judge metric. We report the per-target ASR and the average ASR across all 8 target classes.

5.1.1. Untargeted Attack Setting.

We first validate the scaling laws in the untargeted setting (defined by Eq. 3). To do this, we follow the core experimental settings from Sec. 3.2, using the SSA-CWA algorithm on the same 64-model surrogate pool and NIPS17 dataset. We measure the average ASR against 3 representative target models from Family 1 (Swin-B, ConvNeXt-B, and ResNeXt50). As the untargeted setting is a significantly simpler task, We use a small $\epsilon = 2/255$ to avoid the ASR quickly saturating at 100%, which would obscure the underlying trend. As shown in Fig. 6a, even under untargeted conditions, a clear log-linear trend persists. This confirms that the scaling laws are a general principle of ensemble attacks, independent of the specific attack objective.

5.1.2. Across Different Attack Algorithms.

We now provide a tailored experiment to validate our hypothesis from Sec. 2.2: that the log-linear scaling laws are unlocked only by advanced ensemble optimizers (like CWA or SVRE) that resolve gradient conflict, while naïve ensemble strategies fail to scale.

Experimental Design. To test this, we design two families of attack algorithms and evaluate their scaling performance. All experiments follow the protocol in Sec. 3.2 (targeting *sea lion*) and results are averaged over our standard target classifiers (Family 1 of Sec. 3.2).

- Family 1 (Logit Ensemble Strategies): We test the logit averaging strategy, which we hypothesize will fail to scale. We combine the strategy with various powerful gradient optimizers and input transformations: MI-FGSM [15], DI-MI-FGSM [66], and VMI-FGSM [61].
- Family 2 (Advanced Ensemble Strategies): We then test advanced gradient optimizers. This family includes MI-CWA [8], VMI-CWA [8, 61], and MI-SVRE [68].

Results and Analysis. The results are shown in Fig. 6b. All algorithms in Family 1, which use logit averaging, fail to exhibit the log-linear scaling law. While performance can be boosted by components like DI or VMI, their ASR stagnates at a low value. Conversely, algorithms in Family 2 demonstrate a clear and persistent log-linear scaling law. This behavior mirrors the results of our main SSA-CWA algorithm (from Sec. 3), confirming that the scaling phenomenon is robust across different advanced optimizers,

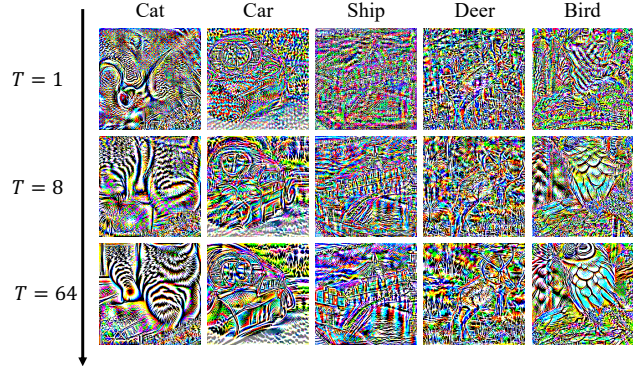


Figure 7. Visualization of adversarial perturbations as T scales. We take 5 labels from CIFAR10 [35] to create adversarial examples as they are relatively easy for human eyes to recognize. As the ensemble cardinality grows (top to bottom), the perturbations evolve from unstructured noise ($T = 1$) into semantically meaningful patterns that resemble features of target classes ($T = 64$).

so long as they resolve the conflict. This experiment confirms our claim: the ability to scale an ensemble attack is contingent on the ensemble optimization strategy.

5.2. The Semantic Nature of Scaled Perturbations

Beyond attack success rates, we investigate *what* the ensemble attack learns as T increases. As shown in Fig. 7, scaling the ensemble fundamentally changes the *nature* of the resulting perturbation. At $T = 1$, the perturbation is noisy and model-specific. However, as T increases to 64, the perturbation evolves to contain clear, interpretable, and semantic features of the target class (e.g., textures for ‘Cat’, an owl-like shape for ‘Bird’).

This is a critical finding that provides a qualitative explanation for the scaling laws. First, scaling T forces the optimizer to discard model-specific, ‘non-robust features’ [32] and instead find a ‘common weakness’ solution that fools all models. Next, our visualization strongly suggests this common weakness is not just a mathematical artifact but is tied to the *semantic essence* of the target class. The attack learns to inject robust features of the target [12].

This reinforces that our scaling approach is a principled method to distill the shared, transferable features of a concept from a diverse set of models. As noted by [22], images

lie on a low-dimensional manifold; our scaling approach appears to provide a more accurate and robust representation of this manifold for the target class.

6. Conclusion

In this work, we investigate scaling laws for black-box adversarial attacks. We find that while gradient conflict stalls naïve ensembling, advanced optimizers (e.g., CWA) unlock a robust log-linear scaling law: the Attack Success Rate increases linearly with $\log T$. We empirically verify this law’s universality across standard classifiers (Sec. 3.3), SOTA defenses, and MLLMs (Sec. 3.4), and show that scaling distills semantic features (Sec. 5.2). Applying this methodology to SOTA MLLMs (Sec. 4) serves as a powerful benchmark. The scaled attack achieves 85.0% ASR on GPT-4o, while Claude-3.5-Sonnet shows exceptional resilience at only 31.0% ASR. Our findings urge a shift in focus for robustness evaluation: from designing intricate algorithms on small ensembles to understanding the principled and powerful threat of scaling, which is crucial for building and verifying genuinely robust foundation models.

References

- [1] Anonymous. TUAP: Targeted universal adversarial perturbations for CLIP. In *Submitted to The Thirteenth International Conference on Learning Representations*, 2024. under review. 2
- [2] Anish Athalye, Nicholas Carlini, and David Wagner. Obfuscated gradients give a false sense of security: Circumventing defenses to adversarial examples. In *International conference on machine learning*, pages 274–283. PMLR, 2018. 14
- [3] Yasaman Bahri, Ethan Dyer, Jared Kaplan, Jaehoon Lee, and Utkarsh Sharma. Explaining neural scaling laws. *Proceedings of the National Academy of Sciences*, 121(27): e2311878121, 2024. 14
- [4] Shuai Bai, Keqin Chen, Xuejing Liu, Jialin Wang, Wenbin Ge, Sibao Song, Kai Dang, Peng Wang, Shijie Wang, Jun Tang, Humen Zhong, Yuanzhi Zhu, Mingkun Yang, Zhaohai Li, Jianqiang Wan, Pengfei Wang, Wei Ding, Zheren Fu, Yiheng Xu, Jiabo Ye, Xi Zhang, Tianbao Xie, Zesen Cheng, Hang Zhang, Zhibo Yang, Haiyang Xu, and Junyang Lin. Qwen2.5-vl technical report, 2025. 5
- [5] Brian R. Bartoldson, James Diffenderfer, Konstantinos Parasyris, and Bhavya Kailkhura. Adversarial robustness limits via scaling-law and human-alignment studies, 2024. 6, 14
- [6] Nicholas Carlini and David Wagner. Towards evaluating the robustness of neural networks. In *2017 IEEE Symposium on Security and Privacy (SP)*, pages 39–57. Ieee, 2017. 14
- [7] Bin Chen, Jiali Yin, Shukai Chen, Bohao Chen, and Ximeng Liu. An adaptive model ensemble adversarial attack for boosting adversarial transferability. In *Proceedings of the IEEE/CVF International Conference on Computer Vision*, pages 4489–4498, 2023. 14
- [8] Huanran Chen, Yichi Zhang, Yinpeng Dong, Xiao Yang, Hang Su, and Jun Zhu. Rethinking model ensemble in transfer-based adversarial attacks. In *The Twelfth International Conference on Learning Representations*, 2024. 2, 3, 4, 8, 12, 14
- [9] Huanran Chen, Yinpeng Dong, Zeming Wei, Hang Su, and Jun Zhu. Towards the worst-case robustness of large language models. *arXiv preprint arXiv:2501.19040*, 2025. 14
- [10] Mehdi Cherti, Romain Beaumont, Ross Wightman, Mitchell Wortsman, Gabriel Ilharco, Cade Gordon, Christoph Schuhmann, Ludwig Schmidt, and Jenia Jitsev. Reproducible scaling laws for contrastive language-image learning. In *Proceedings of the IEEE/CVF Conference on Computer Vision and Pattern Recognition*, pages 2818–2829, 2023. 6, 14
- [11] Gheorghe Comanici, Eric Bieber, Mike Schaekermann, Ice Pasupat, Noveen Sachdeva, Inderjit Dhillon, Marcel Blstein, Ori Ram, Dan Zhang, Evan Rosen, et al. Gemini 2.5: Pushing the frontier with advanced reasoning, multimodality, long context, and next generation agentic capabilities. *arXiv preprint arXiv:2507.06261*, 2025. 6
- [12] Zheng Dai and David Gifford. Fundamental limits on the robustness of image classifiers. In *The Eleventh International Conference on Learning Representations*, 2022. 8
- [13] Thomas G Dietterich. Ensemble methods in machine learning. In *International workshop on multiple classifier systems*, pages 1–15. Springer, 2000. 14
- [14] Yinpeng Dong, Hang Su, Jun Zhu, and Fan Bao. Towards interpretable deep neural networks by leveraging adversarial examples. *arXiv preprint arXiv:1708.05493*, 2017. 1
- [15] Yinpeng Dong, Fangzhou Liao, Tianyu Pang, Hang Su, Jun Zhu, Xiaolin Hu, and Jianguo Li. Boosting adversarial attacks with momentum. In *Proceedings of the IEEE conference on computer vision and pattern recognition*, pages 9185–9193, 2018. 1, 2, 3, 8, 14
- [16] Yinpeng Dong, Tianyu Pang, Hang Su, and Jun Zhu. Evading defenses to transferable adversarial examples by translation-invariant attacks. In *Proceedings of the IEEE/CVF conference on computer vision and pattern recognition*, pages 4312–4321, 2019. 2, 14
- [17] Yinpeng Dong, Qi-An Fu, Xiao Yang, Tianyu Pang, Hang Su, Zihao Xiao, and Jun Zhu. Benchmarking adversarial robustness on image classification. In *Proceedings of the IEEE/CVF Conference on Computer Vision and Pattern Recognition (CVPR)*, pages 321–331, 2020. 5
- [18] Yinpeng Dong, Shuyu Cheng, Tianyu Pang, Hang Su, and Jun Zhu. Query-efficient black-box adversarial attacks guided by a transfer-based prior. *IEEE Transactions on Pattern Analysis and Machine Intelligence*, 44(12):9536–9548, 2021. 14
- [19] Yinpeng Dong, Huanran Chen, Jiawei Chen, Zhengwei Fang, Xiao Yang, Yichi Zhang, Yu Tian, Hang Su, and Jun Zhu. How robust is google’s bard to adversarial image attacks? *arXiv preprint arXiv:2309.11751*, 2023. 2, 7
- [20] Alexey Dosovitskiy. An image is worth 16x16 words: Transformers for image recognition at scale. *arXiv preprint arXiv:2010.11929*, 2020. 4

- [21] Xingwu Sun et al. Hunyuan-large: An open-source moe model with 52 billion activated parameters by tencent, 2024. 14
- [22] Alhussein Fawzi, Hamza Fawzi, and Omar Fawzi. Adversarial vulnerability for any classifier. *Advances in neural information processing systems*, 31, 2018. 8
- [23] Stanislav Fort and Balaji Lakshminarayanan. Ensemble everything everywhere: Multi-scale aggregation for adversarial robustness, 2024. 2
- [24] Lianli Gao, Qilong Zhang, Jingkuan Song, Xianglong Liu, and Heng Tao Shen. Patch-wise attack for fooling deep neural network. In *Computer Vision—ECCV 2020: 16th European Conference, Glasgow, UK, August 23–28, 2020, Proceedings, Part XXVIII 16*, pages 307–322. Springer, 2020. 14
- [25] Raphael Gontijo-Lopes, Yann Dauphin, and Ekin D Cubuk. No one representation to rule them all: Overlapping features of training methods. *arXiv preprint arXiv:2110.12899*, 2021. 14
- [26] Ian J Goodfellow. Explaining and harnessing adversarial examples. *arXiv preprint arXiv:1412.6572*, 2014. 1, 2, 14
- [27] Kaiming He, Xiangyu Zhang, Shaoqing Ren, and Jian Sun. Deep residual learning for image recognition. In *Proceedings of the IEEE conference on computer vision and pattern recognition*, pages 770–778, 2016. 4
- [28] Joel Hestness, Sharan Narang, Newsha Ardalani, Gregory Diamos, Heewoo Jun, Hassan Kianinejad, Md Mostofa Ali Patwary, Yang Yang, and Yanqi Zhou. Deep learning scaling is predictable, empirically. *arXiv preprint arXiv:1712.00409*, 2017. 14
- [29] Gao Huang, Zhuang Liu, Laurens Van Der Maaten, and Kilian Q Weinberger. Densely connected convolutional networks. In *Proceedings of the IEEE conference on computer vision and pattern recognition*, pages 4700–4708, 2017. 4
- [30] Hao Huang, Ziyang Chen, Huanran Chen, Yongtao Wang, and Kevin Zhang. T-sea: Transfer-based self-ensemble attack on object detection. In *Proceedings of the IEEE/CVF conference on computer vision and pattern recognition*, pages 20514–20523, 2023. 14
- [31] Andrew Ilyas, Logan Engstrom, Anish Athalye, and Jessy Lin. Black-box adversarial attacks with limited queries and information. In *International conference on machine learning*, pages 2137–2146. PMLR, 2018. 14
- [32] Andrew Ilyas, Shibani Santurkar, Dimitris Tsipras, Logan Engstrom, Brandon Tran, and Aleksander Madry. Adversarial examples are not bugs, they are features, 2019. 4, 8
- [33] Alex K, Ben Hamner, and Ian Goodfellow. Nips 2017: Non-targeted adversarial attack. <https://kaggle.com/competitions/nips-2017-non-targeted-adversarial-attack>, 2017. Kaggle. 5
- [34] Jared Kaplan, Sam McCandlish, Tom Henighan, Tom B. Brown, Benjamin Chess, Rewon Child, Scott Gray, Alec Radford, Jeffrey Wu, and Dario Amodei. Scaling laws for neural language models, 2020. 2, 14
- [35] Alex Krizhevsky, Geoffrey Hinton, et al. Learning multiple layers of features from tiny images. 2009. 8, 14
- [36] Alex Krizhevsky, Ilya Sutskever, and Geoffrey E Hinton. Imagenet classification with deep convolutional neural networks. *Advances in neural information processing systems*, 25, 2012. 4
- [37] Alexey Kurakin, Ian Goodfellow, and Samy Bengio. Adversarial machine learning at scale. *arXiv preprint arXiv:1611.01236*, 2016. 5
- [38] Christoph H Lampert, Hannes Nickisch, and Stefan Harmeling. Learning to detect unseen object classes by between-class attribute transfer. In *2009 IEEE conference on computer vision and pattern recognition*, pages 951–958. IEEE, 2009. 2
- [39] Yann LeCun, Yoshua Bengio, and Geoffrey Hinton. Deep learning. *nature*, 521(7553):436–444, 2015. 1
- [40] Qizhang Li, Yiwen Guo, Wangmeng Zuo, and Hao Chen. Making substitute models more bayesian can enhance transferability of adversarial examples. *arXiv preprint arXiv:2302.05086*, 2023. 14
- [41] Fangzhou Liao, Ming Liang, Yinpeng Dong, Tianyu Pang, Xiaolin Hu, and Jun Zhu. Defense against adversarial attacks using high-level representation guided denoiser, 2018. 5, 6
- [42] Jiadong Lin, Chuanbiao Song, Kun He, Liwei Wang, and John E Hopcroft. Nesterov accelerated gradient and scale invariance for adversarial attacks. *arXiv preprint arXiv:1908.06281*, 2019. 2, 14
- [43] Haotian Liu, Chunyuan Li, Qingyang Wu, and Yong Jae Lee. Visual instruction tuning, 2023. 5
- [44] Ling Liu, Wenqi Wei, Ka-Ho Chow, Margaret Loper, Emre Gursoy, Stacey Truex, and Yanzhao Wu. Deep neural network ensembles against deception: Ensemble diversity, accuracy and robustness. In *2019 IEEE 16th international conference on mobile ad hoc and sensor systems (MASS)*, pages 274–282. IEEE, 2019. 14
- [45] Yanpei Liu, Xinyun Chen, Chang Liu, and Dawn Song. Delving into transferable adversarial examples and black-box attacks. *arXiv preprint arXiv:1611.02770*, 2016. 1, 2, 14
- [46] Ze Liu, Yutong Lin, Yue Cao, Han Hu, Yixuan Wei, Zheng Zhang, Stephen Lin, and Baining Guo. Swin transformer: Hierarchical vision transformer using shifted windows. In *Proceedings of the IEEE/CVF international conference on computer vision*, pages 10012–10022, 2021. 4
- [47] Zhuang Liu, Hanzi Mao, Chao-Yuan Wu, Christoph Feichtenhofer, Trevor Darrell, and Saining Xie. A convnet for the 2020s. In *Proceedings of the IEEE/CVF conference on computer vision and pattern recognition*, pages 11976–11986, 2022. 5
- [48] Yuyang Long, Qilong Zhang, Boheng Zeng, Lianli Gao, Xianglong Liu, Jian Zhang, and Jingkuan Song. Frequency domain model augmentation for adversarial attack. In *European conference on computer vision*, pages 549–566. Springer, 2022. 2, 3, 12, 14
- [49] Haochen Luo, Jindong Gu, Fengyuan Liu, and Philip Torr. An image is worth 1000 lies: Adversarial transferability across prompts on vision-language models, 2024. 7
- [50] Aleksander Madry. Towards deep learning models resistant to adversarial attacks. *arXiv preprint arXiv:1706.06083*, 2017. 1, 2, 14

- [51] TorchVision maintainers and contributors. Torchvision: Pytorch’s computer vision library. <https://github.com/pytorch/vision>, 2016. 4, 12
- [52] Weili Nie, Brandon Guo, Yujia Huang, Chaowei Xiao, Arash Vahdat, and Anima Anandkumar. Diffusion models for adversarial purification, 2022. 5, 6
- [53] OpenAI. Gpt-4 technical report, 2024. 1, 6
- [54] Mark Palatucci, Dean Pomerleau, Geoffrey E Hinton, and Tom M Mitchell. Zero-shot learning with semantic output codes. *Advances in neural information processing systems*, 22, 2009. 2
- [55] Alec Radford, Jong Wook Kim, Chris Hallacy, Aditya Ramesh, Gabriel Goh, Sandhini Agarwal, Girish Sastry, Amanda Askell, Pamela Mishkin, Jack Clark, Gretchen Krueger, and Ilya Sutskever. Learning transferable visual models from natural language supervision, 2021. 2, 6, 14
- [56] Utkarsh Sharma and Jared Kaplan. Scaling laws from the data manifold dimension. *Journal of Machine Learning Research*, 23(9):1–34, 2022. 14
- [57] C Szegedy. Intriguing properties of neural networks. *arXiv preprint arXiv:1312.6199*, 2013. 1, 2, 14
- [58] Mingxing Tan and Quoc Le. Efficientnet: Rethinking model scaling for convolutional neural networks. In *International conference on machine learning*, pages 6105–6114. PMLR, 2019. 4
- [59] Hugo Touvron, Matthieu Cord, Matthijs Douze, Francisco Massa, Alexandre Sablayrolles, and Hervé Jégou. Training data-efficient image transformers & distillation through attention. In *International conference on machine learning*, pages 10347–10357. PMLR, 2021. 4
- [60] Florian Tramèr, Alexey Kurakin, Nicolas Papernot, Ian Goodfellow, Dan Boneh, and Patrick McDaniel. Ensemble adversarial training: Attacks and defenses. *arXiv preprint arXiv:1705.07204*, 2017. 5
- [61] Xiaosen Wang and Kun He. Enhancing the transferability of adversarial attacks through variance tuning. In *Proceedings of the IEEE/CVF conference on computer vision and pattern recognition*, pages 1924–1933, 2021. 2, 3, 8, 14
- [62] Zeming Wei, Yifei Wang, Ang Li, Yichuan Mo, and Yisen Wang. Jailbreak and guard aligned language models with only few in-context demonstrations. *arXiv preprint arXiv:2310.06387*, 2023. 14
- [63] Ross Wightman. Pytorch image models. <https://github.com/huggingface/pytorch-image-models>, 2019. 4, 12, 14
- [64] Mitchell Wortsman, Gabriel Ilharco, Samir Ya Gadre, Rebecca Roelofs, Raphael Gontijo-Lopes, Ari S Morcos, Hongseok Namkoong, Ali Farhadi, Yair Carmon, Simon Kornblith, et al. Model soups: averaging weights of multiple fine-tuned models improves accuracy without increasing inference time. In *International conference on machine learning*, pages 23965–23998. PMLR, 2022. 14
- [65] Zhiyu Wu, Xiaokang Chen, Zizheng Pan, Xingchao Liu, Wen Liu, Damai Dai, Huazuo Gao, Yiyang Ma, Chengyue Wu, Bingxuan Wang, Zhenda Xie, Yu Wu, Kai Hu, Jiawei Wang, Yaofeng Sun, Yukun Li, Yishi Piao, Kang Guan, Aixian Liu, Xin Xie, Yuxiang You, Kai Dong, Xingkai Yu, Haowei Zhang, Liang Zhao, Yisong Wang, and Chong Ruan. Deepseek-vl2: Mixture-of-experts vision-language models for advanced multimodal understanding, 2024. 6
- [66] Cihang Xie, Zhishuai Zhang, Yuyin Zhou, Song Bai, Jianyu Wang, Zhou Ren, and Alan L Yuille. Improving transferability of adversarial examples with input diversity. In *Proceedings of the IEEE/CVF conference on computer vision and pattern recognition*, pages 2730–2739, 2019. 3, 8, 14
- [67] Saining Xie, Ross Girshick, Piotr Dollár, Zhuowen Tu, and Kaiming He. Aggregated residual transformations for deep neural networks. In *Proceedings of the IEEE conference on computer vision and pattern recognition*, pages 1492–1500, 2017. 5
- [68] Yifeng Xiong, Jiadong Lin, Min Zhang, John E Hopcroft, and Kun He. Stochastic variance reduced ensemble adversarial attack for boosting the adversarial transferability. In *Proceedings of the IEEE/CVF conference on computer vision and pattern recognition*, pages 14983–14992, 2022. 3, 8, 14
- [69] Xiao Yang, Yinpeng Dong, Tianyu Pang, Hang Su, and Jun Zhu. Boosting transferability of targeted adversarial examples via hierarchical generative networks, 2022. 5
- [70] Wei Yao, Zeliang Zhang, Huayi Tang, and Yong Liu. Understanding model ensemble in transferable adversarial attack, 2025. 2, 14
- [71] Chaoning Zhang, Philipp Benz, Tooba Imtiaz, and In-So Kweon. Understanding adversarial examples from the mutual influence of images and perturbations, 2020. 5
- [72] Yechao Zhang, Shengshan Hu, Leo Yu Zhang, Junyu Shi, Minghui Li, Xiaogeng Liu, Wei Wan, and Hai Jin. Why does little robustness help? a further step towards understanding adversarial transferability. In *2024 IEEE Symposium on Security and Privacy (SP)*, pages 3365–3384. IEEE, 2024. 2
- [73] Yichi Zhang, Yao Huang, Yitong Sun, Chang Liu, Zhe Zhao, Zhengwei Fang, Yifan Wang, Huanran Chen, Xiao Yang, Xingxing Wei, Hang Su, Yinpeng Dong, and Jun Zhu. Benchmarking trustworthiness of multimodal large language models: A comprehensive study, 2024. 1, 7, 13
- [74] Yunqing Zhao, Tianyu Pang, Chao Du, Xiao Yang, Chongxuan Li, Ngai-Man Cheung, and Min Lin. On evaluating adversarial robustness of large vision-language models, 2023. 6
- [75] Andy Zou, Zifan Wang, Nicholas Carlini, Milad Nasr, J Zico Kolter, and Matt Fredrikson. Universal and transferable adversarial attacks on aligned language models. *arXiv preprint arXiv:2307.15043*, 2023. 14

A. Proof of Theorem 1.

As defined in Definition 1, \mathbf{x}^* is the minimizer of the population loss $\mathbb{L}(\mathbf{x}) = \mathbb{E}_{f \in \mathcal{F}}[\mathcal{L}(f(\mathbf{x}), \mathbf{y})]$, and $\hat{\mathbf{x}}$ is the minimizer of the empirical loss $\hat{\mathbb{L}}(\mathbf{x}) = \frac{1}{T} \sum_{i=1}^T \mathcal{L}(f_i(\mathbf{x}), \mathbf{y})$. Thereby we have by gradient equals 0:

$$\nabla \mathbb{L}(\mathbf{x}^*) = \nabla \hat{\mathbb{L}}(\hat{\mathbf{x}}) = 0$$

We use Taylor expansion of $\nabla \hat{\mathbb{L}}$ at $\hat{\mathbf{x}}$:

$$0 = \nabla \hat{\mathbb{L}}(\hat{\mathbf{x}}) = \nabla \hat{\mathbb{L}}(\mathbf{x}^*) + \nabla^2 \hat{\mathbb{L}}(\mathbf{x}^*)(\hat{\mathbf{x}} - \mathbf{x}^*) + \mathcal{O}(\|\hat{\mathbf{x}} - \mathbf{x}^*\|^2).$$

Rearranging, we have:

$$\sqrt{T}(\hat{\mathbf{x}} - \mathbf{x}^*) \approx -\sqrt{T}(\nabla^2 \hat{\mathbb{L}}(\mathbf{x}^*))^{-1} \nabla \hat{\mathbb{L}}(\mathbf{x}^*).$$

From Central Limit Theorem:

$$\begin{aligned} \sqrt{T} \nabla \hat{\mathbb{L}}(\mathbf{x}^*) &= \sqrt{T}(\nabla \hat{\mathbb{L}}(\mathbf{x}^*) - \nabla \mathbb{L}(\mathbf{x}^*)) \\ &\stackrel{d}{\rightarrow} \mathcal{N}(0, \text{Cov}(\mathbb{L}(f_i(\mathbf{x}^*)))), \end{aligned}$$

and the law of large numbers:

$$\nabla^2 \hat{\mathbb{L}}(\mathbf{x}^*) \xrightarrow{P} \nabla^2 \mathbb{L}(\mathbf{x}^*).$$

Plug into the previous equation using $\mathcal{AN}(0, \Sigma) = \mathcal{N}(0, A\Sigma A^T)$:

$$\begin{aligned} \sqrt{T}(\hat{\mathbf{x}} - \mathbf{x}^*) &\stackrel{d}{\rightarrow} (\nabla^2 \mathbb{L}(\mathbf{x}^*))^{-1} \mathcal{N}(0, \text{Cov}(\mathbb{L}(f_i(\mathbf{x}^*)))) \\ &\stackrel{d}{=} \mathcal{N}(0, \nabla^2 \mathbb{L}(\mathbf{x}^*)^{-1} \text{Cov}(\mathbb{L}(f_i(\mathbf{x}^*))) \nabla^2 \mathbb{L}(\mathbf{x}^*)^{-1}). \end{aligned}$$

The above indicate $\hat{\mathbf{x}} - \mathbf{x}^*$ converges in $\mathcal{O}(\frac{1}{\sqrt{T}})$.

We can also use Taylor expansion of \mathbb{L} at \mathbf{x}^* :

$$\mathbb{L}(\hat{\mathbf{x}}) \approx \mathbb{L}(\mathbf{x}^*) + 0 + \frac{1}{2}(\hat{\mathbf{x}} - \mathbf{x}^*)^T \nabla^2 \mathbb{L}(\mathbf{x}^*)(\hat{\mathbf{x}} - \mathbf{x}^*).$$

Rearranging, we have:

$$\begin{aligned} T(\mathbb{L}(\hat{\mathbf{x}}) - \mathbb{L}(\mathbf{x}^*)) &\approx \frac{1}{2} \sqrt{T}(\hat{\mathbf{x}} - \mathbf{x}^*)^T \nabla^2 \mathbb{L}(\mathbf{x}^*) \sqrt{T}(\hat{\mathbf{x}} - \mathbf{x}^*) \\ &= \frac{1}{2} \|\nabla^2 \mathbb{L}(\mathbf{x}^*) \sqrt{T}(\hat{\mathbf{x}} - \mathbf{x}^*)\|_2^2 = \frac{1}{2} \|S\|_2^2, \end{aligned}$$

where

$$S \sim \mathcal{N}(0, \nabla^2 \mathbb{L}(\mathbf{x}^*)^{-1/2} \text{Cov}(\mathbb{L}(f_i(\mathbf{x}^*))) \nabla^2 \mathbb{L}(\mathbf{x}^*)^{-1/2}).$$

Thus $T(\mathbb{L}(\hat{\mathbf{x}}) - \mathbb{L}(\mathbf{x}^*))$ converges into a chi-square distribution, which means $\mathbb{L}(\hat{\mathbf{x}}) - \mathbb{L}(\mathbf{x}^*)$ converges in $\mathcal{O}(\frac{1}{T})$.

B. Experiment Settings for Scaling Laws

In this section we list our models that are included in Sec. 3.2. We select these models based on their diversity in architectures, training methods, and training datasets. Results are shown in Table 2 and Table 3, where all of our models come from open-source platforms such as Torchvision [51] and Timm [63]. Note that *default* in the table means normally trained on ImageNet-1K dataset.

Model name	Architecture	Settings
AlexNet	alexnet	default
DenseNet	densenet121 densenet161 densenet169	default default default
EfficientNet	efficientnet-b0 efficientnet-b1 efficientnet-b4 efficientnet-v2-s efficientnet-v2-m efficientnet-v2-l	default default default default default default
GoogleNet	googlenet	default
Inception	inception-v3	default
MaxVit	maxvit-t	default
MnasNet	mnasnet-0-5 mnasnet-0-75 mnasnet-1-0 mnasnet-1-3	default default default default
MobileNet	mobilenet-v2 mobilenet-v3-s mobilenet-v3-l	default default default
RegNet	regnet-x-8gf regnet-x-32gf regnet-x-400mf regnet-x-800mf regnet-y-16gf regnet-y-32gf regnet-y-400mf regnet-y-800mf	default default default default default default default default
ResNet	resnet18 resnet34 resnet50 resnet101 resnet152	default default default default default
ShuffleNet	shufflenet-v2-x0.5 shufflenet-v2-x1.0 shufflenet-v2-x1.5 shufflenet-v2-x2.0	default default default default
SqueezeNet	squeezenet-1.0 squeezenet-1.1	default default
ViT	vit-b-16 vit-b-32 vit-l-16 vit-l-32 vit-b-16	default default default default pretrained on ImageNet-21K

Table 2. List of pretrained image classifiers that are selected for our model ensemble.

C. SSA-CWA Algorithm Declaration

We provide the pseudo-code version of SSA-CWA implementation in Algorithm 1. Their combination is induced from [48] and [8], while implementations of other algorithms (e.g., MI-FGSM, MI-CWA) can be found in their

Model name	Architecture	Settings
Vgg	vgg11	default
	vgg11-bn	default
	vgg13	default
	vgg13-bn	default
	vgg16	default
	vgg16-bn	default
	vgg19	default
Wide-ResNet	wide-resnet50-2	default
	wide-resnet101-2	default
BeiT	beit-B-16	pretrained on ImageNet-21k
GhostNet	ghostnet-100	default
DeiT	deit-B-16	default
LCnet	lcnet-050	default
RepVgg	repvgg-a2	default
DPN	dpn98	default
SegFormer	mit-b0	default
BiT	bit-50	default
CvT	cvt-13	default
Twins-SVT	twins-svt-large	default
NFNet	nfnet-10	default

Table 3. List of pretrained image classifiers that are selected for our model ensemble (continued).

corresponding papers.

Algorithm 1 SSA-CWA Algorithm

- 1: **Input:** natural image \mathbf{x}_{nat} , label \mathbf{y} , L_∞ constraint ϵ , iterations T , loss function \mathcal{L} , spectrum transformation function \mathcal{T} , model ensemble $\{f_i\}_{i=1}^N$, spectrum transformation times M , decay factor μ , step sizes α, β .
- 2: **Output:** An adversarial example \mathbf{x}
- 3: **for** $t = 0$ **to** $T-1$ **do**
- 4: Update \mathbf{x}_t by $\mathbf{x}_t^0 = \mathbf{x}_{t-1}$
- 5: **for** $i = 1$ **to** N **do**
- 6: **for** $j = 1$ **to** M **do** ▷ Spectrum transformation
- 7: Obtain transformed image $\mathcal{T}(\mathbf{x}_{t,i}^j)$
- 8: Compute $\mathbf{g}_i^j = \nabla_{\mathbf{x}_{t,i}^j} \mathcal{L}(\mathcal{T}(\mathbf{x}_{t,i}^j), \mathbf{y})$
- 9: **end for**
- 10: Compute gradient $\mathbf{g}_i = \frac{1}{M} \sum_{j=1}^M \mathbf{g}_i^j$
- 11: Update inner momentum by $\mathbf{m} = \mu \cdot \mathbf{m} + \frac{\mathbf{g}_i}{\|\mathbf{g}_i\|_2}$
- 12: Update $\mathbf{x}_t^i = \text{clip}(\mathbf{x}_{\text{nat}}, \epsilon) \{ \mathbf{x}_t^{i-1} + \beta \cdot \mathbf{m} \}$
- 13: **end for**
- 14: Compute gradient $\mathbf{g} = \mathbf{x}_t^N - \mathbf{x}_t^0$
- 15: Update outer momentum by $\mathbf{h} = \mu \cdot \mathbf{h} + \frac{\mathbf{g}}{\|\mathbf{g}\|_2}$
- 16: $\mathbf{x}_t = \text{clip}(\mathbf{x}_{\text{nat}}, \epsilon) \{ \mathbf{x}_t^N + \alpha \cdot \text{sign}(\mathbf{h}) \}$
- 17: **end for**
- 18: **Return:** \mathbf{x}_{T-1}

D. Evaluation Metrics Details

As MLLMs output generative text rather than classification logits, assessing attack success requires parsing natural language descriptions. In this work, we employ two distinct evaluation paradigms tailored to the specific experimental goals in Sec. 3 and Sec. 4.

In Sec. 3.4.2 (Family 3: MLLMs), we evaluate the scaling laws using a string-matching approach. Since MLLMs often produce descriptive text rather than the precise ImageNet class names, strict exact matching can lead to false negatives. Therefore, we adopt a relaxed keyword map. An attack is considered successful if the MLLM’s output contains any of the keywords associated with the target label.

Table 4 lists the target labels used in our experiments and their corresponding relaxed keywords.

Target Label (ImageNet)	Accepted Keywords (Case-Insensitive)
Sea Lion	sea lion, seal, marine mammal
Barometer	barometer, gauge, measuring instrument, clock
Swing	swing, playground, seat
Pickelhaube	pickelhaube, helmet, spiked helmet, military hat
Fig	fig, fruit, plant
Lock	lock, padlock, dial
Computer	computer, pc, laptop, desktop, phone, device
Snake	snake, serpent, reptile, python, cobra

Table 4. The relaxed keyword map used for evaluating MLLMs in Sec. 3. We map the specific ImageNet class label to a set of semantically equivalent or broader keywords.

In Sec. 4, to rigorously benchmark SOTA MLLMs, we adopt the LLM-as-Judge framework inspired by MultiTrust [73]. We use GPT-4o as the judge to evaluate the quality and success of the attack.

The evaluation is strict: an attack is successful *only if* the description mentions the target and does not mention artifacts of the attack (noise, distortion). Fig. 8 presents the exact system prompt used in our experiments.

Prompt for GPT-4o Judge Correctness:
Given a chatbot’s description of a scene: [response].
If it is stated in the description that there is a/an [label]? Please answer ‘Yes.’ or ‘No.’.

Prompt for GPT-4o Judge Image Quality:
Given a chatbot’s description of an image: [response]. Does the description mention factors that affect the judgment of the image content, such as low image quality, noise, or modification? Please answer ‘Yes.’ or ‘No.’.

Figure 8. The GPT-4o system prompt used for the unified evaluation metric in Sec. 4. This metric ensures that successful attacks are both effective (semantics changed) and stealthy (no obvious noise detected by the model).

E. Experiment Settings for Attacking MLLMs

Model Name	Architecture	Datasets
ViT-L OpenAI	ViT-L-14	WebImageText
ViT-B LAION-2B	ViT-B-32	LAION-2B
ViT-B LAION-2B	ViT-B-16	LAION-2B
ViT-bigG LAION-2B	ViT-bigG-14	LAION-2B
ViT-g LAION-2B	ViT-g-14	LAION-2B
ViT-H LAION-2B	ViT-H-14	LAION-2B
ViT-L LAION-2B	ViT-L-14	LAION-2B
ConvNeXt-L LAION-2B	ConvNeXt-large-d-320	LAION-2B
ViT-B DataComp	ViT-B-16	DataComp-1B
ViT-B DataComp	ViT-B-32	DataComp-1B
ViT-L DataComp	ViT-L-14	DataComp-1B
SigLip WebLI	ViT-SO400M-14-SigLIP	WebLI

Table 5. List of CLIPs that are selected as model ensemble.

In Table. 5 we list the 12 CLIPs that are collected for our model ensemble, which are all open-source models selected from OpenAI [55], OpenCLIP [10], and Timm [63].

F. Related Work

F.1. Black-Box Attacks

Deep learning models are widely recognized for their vulnerability to adversarial attacks [26, 57]. Extensive research has documented this susceptibility, particularly in image classification contexts [2, 6], under two principal settings: white-box and black-box attacks. In the white-box setting, the adversary has complete access to the target model [50]. Conversely, in the black-box setting, such information is obscured from the attacker. With limited access to the target model, black-box attacks typically either construct queries and rely on feedback from the model [18, 31] or leverage the transferability of predefined surrogate models [45]. Query-based attacks often suffer from high time complexity and substantial computational costs, making transfer-based methods more practical and cost-effective for generating adversarial examples, as they do not necessitate direct interaction with target models during the training phase.

Within the realm of transfer-based attacks, existing methods can generally be categorized into three types: input transformation, gradient-based optimization, and ensemble attacks. Input transformation methods employ data augmentation techniques before feeding inputs into models, such as resizing and padding [66], translations [16], or transforming them into frequency domain [48]. Gradient-based methods concentrate on designing optimization algorithms to improve transferability, incorporating strategies such as momentum optimization [15, 42], scheduled step sizes [24], and gradient variance reduction [61].

F.2. Ensemble Attacks

Inspired by model ensemble techniques in machine learning [13, 25, 64], researchers have developed sophisticated adversarial attack strategies utilizing sets of surrogate models. In forming an ensemble paradigm, practitioners often average over losses [15], predictions [45], or logits [15]. Additionally, advanced ensemble algorithms have been proposed to enhance adversarial transferability [7, 8, 40, 68]. However, these approaches tend to treat model ensemble as a mere technique for improving transferability without delving into the underlying principles.

Prior studies [30] indicate that increasing the number of classifiers in adversarial attacks can effectively reduce the upper bound of generalization error in Empirical Risk Minimization. Recent research [70] has theoretically defined transferability error and sought to minimize it through model ensemble. Nonetheless, while an upper bound is given, they do not really scale up in practice and have to train neural networks from scratch to meet the assumption of sufficient diversity among ensemble models [44].

F.3. Scaling Laws

In recent years, the concept of scaling laws has gained significant attention. These laws describe the relationship between model size – measured in terms of parameters, data, or training FLOPs – and generalization ability, typically reflected in evaluation loss [34]. Subsequent studies have expanded on scaling laws from various perspectives, including image classification [3, 28], language modeling [56] and mixture of experts (MoE) models [21], highlighting the fundamental nature of this empirical relationship.

In the domain of adversarial attack research, recent work has attempted to derive scaling laws for adversarially trained defense models on CIFAR-10 [5, 35]. However, the broader concept of scaling remains underexplored. While some preliminary observations on the effect of enlarging model ensembles can be found in prior studies [70], these effects have not been systematically analyzed. Recent work Wei et al. [62] also explore the scaling law of attack success rate when jailbreaking large language models [9, 75] by increasing number of in-context demonstrations. In this paper, however, we focus on the empirical scaling laws within model ensembles, and verify it through extensive experiments on open-source pretrained models. Motivated by this perspective, we unveil vulnerabilities within commercial LLMs by targeting their vision encoders.